Q. J. R. Meteorol. Soc. (2002), **128**, pp. 2129–2144

Error analysis of TMI rainfall estimates over ocean for variational data assimilation

By PETER BAUER[1*], JEAN-FRANÇOIS MAHFOUF[1], WILLIAM S. OLSON[2], FRANK S. MARZANO[3], SABATINO DI MICHELE[4], ALESSANDRA TASSA[4] and ALBERTO MUGNAI[4]

[1] *European Centre for Medium-Range Weather Forecasts, UK*
[2] *Joint Center for Earth Systems Technology, USA*
[3] *Università dell'Aquila, Italy*
[4] *Istituto di Fisica dell'Atmosfera, Italy*

(Received 22 October 2001; revised 12 April 2002)

SUMMARY

An intercomparison of retrieval errors from different Tropical Rainfall Measuring Mission (TRMM) passive microwave rainfall products was carried out to assess the definition of observation error for experiments of rainfall assimilation in a variational framework. Depending on algorithms and their spatial resolution and sampling, a large variety of error estimates occurred. The error propagation to the European Centre for Medium-Range Weather Forecasts (ECMWF) model grid (here 45 and 60 km) was investigated from error simulations and observed data with and without accounting for spatial error correlation.

All algorithms used in this study (TRMM standard product 2A12 V.5 and two alternative algorithms, namely PATER and BAMPR) employ a Bayesian retrieval framework. The Bayesian errors obtained from each algorithm from different case-studies showed values well above 100% at low rain rates (0.1 mm h^{-1}) and around 50% at high rain rates (20–50 mm h^{-1}) at the original product resolution and sampling. These Bayesian errors corresponded very well with those from an independent evaluation which was carried out by comparing TRMM microwave radiometer (TMI) estimates to precipitation radar retrievals at the same (here $\approx 27 \times 40$ km^2) resolution.

The impact of spatial averaging on retrieval errors was simulated using fits to the Bayesian errors and realistic log-normal rainfall probability distributions. By neglecting spatial correlation, the range of errors is reduced from 70–200% to 20–50% at low rain rates and from 25–70% to 5–20% at high rain rates. To account for spatial data correlation, TMI observations were first averaged to the ECMWF model grid. Then the decorrelation of rain rates as a function of separation distance from all products was calculated. The introduction of spatial error correlation affected both error reduction and dispersion of errors per rain-rate interval. The final error estimates ranged from 50–150% at low rain rates to 20–50% at high rain rates. The analysis suggests that once the spatial correlation pattern of a product is known, the probability density distribution of real observations inside the model grid does not produce larger scatter and therefore a simple scaling may suffice to calculate rainfall retrieval errors at the model resolution.

KEYWORDS: Bayesian retrieval Retrieval errors Spatial correlation TRMM

1. INTRODUCTION

Assimilation of observations into numerical weather prediction (NWP) models requires knowledge of both systematic and random errors in the observations. Systematic observation errors, once identified, are corrected through bias correction schemes assuming that the model output is unbiased. Random errors are included in both background- and observation-error covariance matrices and represent how much weight is given to model first-guess or observation in the assimilation procedure. Even though rainfall retrieval errors are known to be rather large, they may still provide useful information within an assimilation system since the model background errors will be of similar magnitude.

Following rainfall assimilation experiments in a three-dimensional assimilation system (Treadon 1997), the first attempt to exploit the impact of the assimilation of rainfall data obtained from satellite measurements on analysis and forecast in an operational four-dimensional variational assimilation system (e.g. Rabier *et al.* 2000) was conducted for the EuroTRMM project (e.g. Marécal and Mahfouf 2000, 2002) using

* Corresponding author: ECMWF, Shinfield Park, Reading, Berkshire RG2 9AX, UK.
e-mail: peter.bauer@ecmwf.int

TABLE 1. ALGORITHM SPECIFICATIONS

Algorithm	Reference	Resolution (km^2)	Sampling cross-track/along-track	Sensors
PATER	Bauer *et al.* (2001)	27×44	10 km/14 km	TMI (PR)
BAMPR	Mugnai *et al.* (2000)	10×16	10 km/14 km	TMI (PR)
2A12	Kummerow *et al.* (1996)	10×16	5 km/14 km	TMI

See text for details of abbreviations.

observations from the Tropical Rainfall Measuring Mission (TRMM) (Kummerow *et al.* 1998). Part of this effort was the investigation of model sensitivity to data product (i.e. retrieval algorithm) and to associated errors (Marécal *et al.* 2002).

For this purpose, two new algorithms have been developed: (i) Precipitation Radar (PR) Adjusted TRMM Microwave Radiometer (TMI) Estimation of Rainfall (PATER) (Bauer *et al.* 2001), and (ii) Bayesian Algorithm for Microwave-based Precipitation Retrieval (BAMPR) (Mugnai *et al.* 2001). Both methods allow the inclusion of PR data for constraining the primary TMI retrievals but only TMI retrievals will be analysed here. These algorithms were compared to the TRMM standard product 2A12 that contains hydrometeor profiles retrieved from TMI data employing the algorithm proposed by Kummerow *et al.* (1996). Depending on the algorithm, the errors were defined differently as a product of both the employed inversion procedure and the training datasets. Algorithms and errors are compiled in sections 2 and 3.

This paper summarizes the error definition for these algorithms and how they may be used within a variational assimilation system. Apart from their quantitative differences, these errors depend on (i) the data used for training the algorithm and (ii) the geometrical layout, i.e. spatial resolution and sampling of the final product. The first issue includes errors introduced by radiative-transfer simulations based on hydrometeor profiles which do not well represent the observed ones; errors in the assumed particle size distributions; their composition and shape as well as insufficient surface emissivity modelling; errors associated with the numerical solution to the radiative-transfer problem in scattering atmospheres; and radiometer noise. The order in this list roughly corresponds to the magnitude of the contribution from each element to the total error. General information on all three algorithms is summarized in Table 1.

The usage of retrieval products of this kind in global models requires a scaling to the model grid resolution. Our work presents a procedure to unify the errors at the spatial resolution of two versions of the European Centre for Medium-Range Weather Forecasts (ECMWF) model, that is T_L319 (truncation to a linear grid with wavenumber 319) and T_L511 which correspond to $\approx$60 km and $\approx$45 km grid-box sizes. This scaling is carried out in a general way, neglecting spatial error correlation and by inclusion of spatial error correlation using both idealized rainfall probability distributions and real data. These two approaches are described in section 4.

Another motivation for our study was the stimulation of further investigations on retrieval-error estimation in the framework of satellite rainfall data assimilation in preparation for its operational use at NWP centres. With the increasing computational efficiency of global models, the assimilation of new remote-sensing data becomes feasible. Please note that this paper does not address the accuracy of the forecast model. Secondly, all problems related to temporal sampling errors, i.e. the errors resulting from limited satellite data coverage per grid box over the assimilation window, are not addressed.

2. BAYESIAN RETRIEVAL

The Bayesian retrieval framework (e.g. Lorenc 1986) is the basis for all algorithms used in this study so that it is only briefly summarized at this point. It makes use of the probabilities P of observations $\mathbf{y}^{\mathrm{o}}$ (here in terms of brightness temperature vectors **TB**) and atmospheric states (in terms of hydrometeor profiles or their reduction to surface rain rate $\mathbf{x}$) due to the inherent estimate uncertainty that $\mathbf{x}$ always produces $\mathbf{y}^{\mathrm{o}}$. $P(\mathbf{x})$ is the a priori probability of $\mathbf{x}$ while $P(\mathbf{y}^{\mathrm{o}})$ is the probability that observation $\mathbf{y}^{\mathrm{o}}$ occurs. $P(\mathbf{y}^{\mathrm{o}}|\mathbf{x})$ is the conditional probability that $\mathbf{y}^{\mathrm{o}}$ can be measured for atmospheric state $\mathbf{x}$ whereas $P(\mathbf{x}|\mathbf{y}^{\mathrm{o}})$ is the conditional probability that atmospheric state $\mathbf{x}$ is present once $\mathbf{y}^{\mathrm{o}}$ is observed.

$P(\mathbf{x}, \mathbf{y}^{\mathrm{o}})$ describes the common probability that atmospheric state $\mathbf{x}$ is present and observation $\mathbf{y}^{\mathrm{o}}$ is made. The joint probability is

$$P(\mathbf{x}, \mathbf{y}^{\mathrm{o}}) = P(\mathbf{x}|\mathbf{y}^{\mathrm{o}})P(\mathbf{y}^{\mathrm{o}}) = P(\mathbf{y}^{\mathrm{o}}|\mathbf{x})P(\mathbf{x}), \tag{1}$$

which leads to the Bayes rule for the a posteriori probability

$$P(\mathbf{x}|\mathbf{y}^{\mathrm{o}}) = \frac{P(\mathbf{y}^{\mathrm{o}}|\mathbf{x})P(\mathbf{x})}{P(\mathbf{y}^{\mathrm{o}})}. \tag{2}$$

In the case of rainfall retrievals, $P(\mathbf{x})$ originates from the a priori knowledge on cloud variability and is usually taken from cloud-resolving model simulations.

$P(\mathbf{y}^{\mathrm{o}}|\mathbf{x})$ may be transformed to $P(\mathbf{y}^{\mathrm{o}} - \mathbf{y}(\mathbf{x}))$ which is the probability of the deviations of the observations $\mathbf{y}^{\mathrm{o}}$ from synthetic observations $\mathbf{y}(\mathbf{x})$ obtained from state $\mathbf{x}$ using a radiative-transfer model. This departure is sensitive to both observation and radiative-transfer modelling errors. Assuming that $P(\mathbf{y}^{\mathrm{o}} - \mathbf{y}(\mathbf{x}))$ is a multi-dimensional Gaussian function and that observation and radiative-transfer errors are uncorrelated (Lorenc 1986),

$$P(\mathbf{y}^{\mathrm{o}} - \mathbf{y}(\mathbf{x})) \propto \exp\left\{-\tfrac{1}{2}(\mathbf{y}^{\mathrm{o}} - \mathbf{y}(\mathbf{x}))^{\mathrm{T}}(\mathbf{E}+\mathbf{F})^{-1}(\mathbf{y}^{\mathrm{o}} - \mathbf{y}(\mathbf{x}))\right\}, \tag{3}$$

where $(\mathbf{E}+\mathbf{F})$ are the covariance matrices of observation (i.e. instrument noise) and modelling errors.

The best estimate of atmospheric state (i.e. the analysis $\mathbf{x}_{\mathrm{a}}$) may be produced from the expected value which is identical to the minimum variance solution in this context:

$$\mathbf{x}_{\mathrm{a}} = \int \mathbf{x}P(\mathbf{x}|\mathbf{y}^{\mathrm{o}})\,\mathrm{d}\mathbf{x} \propto \int P(\mathbf{y}^{\mathrm{o}} - \mathbf{y}(\mathbf{x}))P(\mathbf{x})\mathbf{x}\,\mathrm{d}\mathbf{x}. \tag{4}$$

Alternatively, a maximum a posteriori probability approach can be chosen where $\mathbf{x}_{\mathrm{a}} = \max P(\mathbf{y}^{\mathrm{o}} - \mathbf{y}(\mathbf{x}))P(\mathbf{x})$ (e.g. Marzano *et al.* 1999).

Again, for less ill-conditioned retrieval problems, the deviation from the background state has to be accounted for in (4) and iterative optimization towards the smallest deviations in observable and state space is then performed. In the case of precipitation retrievals, the optimization is likely to fail due to the large number of unknowns. Therefore, $P(\mathbf{x})$ enters the integration through the relative number of profiles contained in an off-line database. This database is usually obtained from mesoscale cloud model simulations because these provide consistent three-dimensional hydrometeor distributions (Olson *et al.* 1996). Of course, the lack of representativeness of these simulations may cause serious problems in the evaluation of (4) (Bauer 2001). Under the assumption of realistic $P(\mathbf{x})$, a way to numerically calculate (4) is given by (Olson *et al.* 1996):

$$\mathbf{x}_{\mathrm{a}} = \frac{\sum_i J^{\mathrm{o}}(\mathbf{y}^{\mathrm{o}}, \mathbf{y}(\mathbf{x}_i))\mathbf{x}_i}{\sum_i J^{\mathrm{o}}(\mathbf{y}^{\mathrm{o}}, \mathbf{y}(\mathbf{x}_i))}, \tag{5}$$

with cost function J^{o}:

$$J^{\mathrm{o}}(\mathbf{y}^{\mathrm{o}}, \mathbf{y}(\mathbf{x}_i)) = \exp\{-\tfrac{1}{2}(\mathbf{y}^{\mathrm{o}} - \mathbf{y}(\mathbf{x}_i))^{\mathrm{T}}(\mathbf{E} + \mathbf{F})^{-1}(\mathbf{y}^{\mathrm{o}} - \mathbf{y}(\mathbf{x}_i))\},$$

and where $\mathbf{x}_i$ represents an individual state profile in the database. To be exact, the modelling errors $\mathbf{F}$ should be quantified for each $\mathbf{x}_i$; however, this would require the knowledge of the dependence of radiative-transfer errors on local hydrometeor profiles. The inherent uncertainty is given by the integration of analysis values from those contained in the database:

$$\sigma_{\mathrm{a}}^2 = \frac{\sum_i J^{\mathrm{o}}(\mathbf{y}^{\mathrm{o}}, \mathbf{y}(\mathbf{x}_i))(\mathbf{x}_i - \mathbf{x}_{\mathrm{a}})^2}{\sum_i J^{\mathrm{o}}(\mathbf{y}^{\mathrm{o}}, \mathbf{y}(\mathbf{x}_i))}. \tag{6}$$

It has to be noted that this error estimate is subject to the representativeness of the database and the assumptions made for observation and modelling errors.

3. ALGORITHMS

(*a*) *PATER*

The PATER algorithm employs a comprehensive set of cloud-resolving model simulations where the final retrieval database contains only those hydrometeor profiles whose simulated brightness temperatures $\mathbf{y}(\mathbf{x}_i)$, were found in a large set of TMI observations. This was carried out to ensure improved representativeness in terms of the assumptions made between (4) and (5). Also, (5) was defined using only two empirical orthogonal functions, instead of nine brightness temperatures, without any constraints on the retrieval, and without using the 85.5 GHz channels. It is important to note that this algorithm yields rainwater content (w in g m^{-3}) rather than rain rate (RR in mm h^{-1}); for conversion, the relation $RR = 20.95w^{1.12}$ has been used. The error of this fit is well below 1% for $w \in [0, 2$ g m$^{-3}]$ and a gamma drop size distribution with a shape parameter of one.

(*b*) *BAMPR*

BAMPR is based on the retrieval scheme implemented by Marzano *et al.* (1999) of which the radiometer-only version was used here (Mugnai *et al.* 2001). As for PATER and 2A12, selected mesoscale simulations were combined for database construction and the Bayesian framework represents the retrieval part. The radiative transfer was applied to slanted hydrometeor columns at cloud model resolution along the TMI viewing angle. The simulated TBs were then convolved using TMI footprint dimensions. An additional feature of BAMPR is the adjustment of raindrop size distributions in situations where insufficient matches between simulations and observations occur since these were identified as the main error source in the BAMPR simulation databases by Panegrossi *et al.* (1998). The database was subdivided into less and more intense rainfall regimes. Thus, the inversion employs a scene identification before the inversion methodology itself is applied. A minimum variance scheme was adopted without limiting assumptions on error and a priori probability distributions.

(*c*) *2A12*

The TRMM standard TMI algorithm 2A12 is based on the Goddard Profiling Algorithm which was developed for applications to aircraft data and later to satellite data from the Special Sensor Microwave/Imager (Kummerow *et al.* 1996; Olson *et al.* 1996). The referenced articles also describe the cloud model simulations contained in the database; i.e. represented by all $P(\mathbf{x})$. It employs the solution given in section 2 where $\mathbf{y}^{\mathrm{o}}$ contains **TB** as well as emission/scattering indices. It also uses constraints derived from stratiform-convective classification and distance-from-convection measures (Kummerow *et al.* 2001). The latter have been introduced between versions 4 and 5.

4. Errors

From PATER, two independent uncertainty estimates may be obtained. The first is the 'Bayesian' error from (6). Since PATER employs empirical orthogonal functions, the sum of errors in (5) is replaced: $(\mathbf{E}+\mathbf{F})^{-1}$ becomes $\{\mathbf{E}_{\mathrm{s}}(\mathbf{E}+\mathbf{F})\mathbf{E}_{\mathrm{s}}^{\mathrm{T}}\}^{-1}$ where $\mathbf{E}_{\mathrm{s}}$ denotes the eigenvector matrix associated with the simulations. Radiative-transfer errors are assumed to be (2, 4, 4, 6 K) at (10.65, 19.35, 21.3, 37.0 GHz). The second error estimate originates from the intercomparison of PR and TMI estimates of near-surface rain liquid-water contents at the same resolution (Bauer *et al.* 2001). It can be shown that, in the range of 1–15 mm h^{-1}, this error is mostly driven by the database ambiguity that is the standard deviation of multiple solutions having the same TB-signature (Bauer 2001). For lower rain rates, the background noise originating from surface, non-precipitating clouds and atmosphere supersedes the rain signal, while for rain rates above 15 mm h^{-1} the signature from precipitating ice reduces the contribution of rainwater to the signal. Both background noise and extreme precipitation are less well represented in the databases because (i) surface and clear-sky variability is limited, and (ii) ice microphysics parametrizations are less accurate in the available cloud model simulations so that the 'Bayesian' error estimate will be worse than in moderate situations.

The BAMPR error covariances, i.e. $(\mathbf{E}+\mathbf{F})$ in (6), were derived from sensitivity tests. For this purpose, reference parameters such as the slope of particle size distributions, the presence of melting particles, sea surface wind speed, approximations to radiative-transfer modelling, the temperature profile, and field-of-view dimensions were randomly varied within a given range. The resulting TBs were compared to those from the reference configuration, and the statistics of these errors were computed (Tassa *et al.* 2002).

Since the 2A12 version 5 (V.5) products contained no error information, a rough estimate of 25% on the 60 km model grid (Kummerow 1999, personal communication) was used in the previously mentioned assimilation studies. In preparation for version 6, however, an explicit error estimate through usage of (6) was implemented with an updated version of 2A12 V.5 (called V5.1 hereafter while the official release VH6 may still contain further updates).

Figure 1 shows examples of these errors collected from several cases which are listed in Table 2. Comparing the results in Fig. 1, it is noted that, despite the different approaches used for the error calculation and the different magnitudes of modelling errors assumed for $\mathbf{E}+\mathbf{F}$, the gross behaviour of all algorithms is fairly similar. For moderate rainfall rates, i.e. between 1 and 20 mm h^{-1}, errors decrease from $\approx$100% to $\approx$50%. This represents the range where the signal-to-noise ratio is best because surface effects are suppressed by the rather large cloud opacity, while extreme events with large cloud ice contents occur predominantly in more intense systems. The errors also suggest that the variability of cloud-resolving model profiles used by all algorithms is fairly similar. Since the non-uniqueness of the TB–rainfall relationship is the major error source in this range, the contribution of modelling errors to (6) is rather small. Therefore, the accurate error estimation requires the analysis of both cloud model

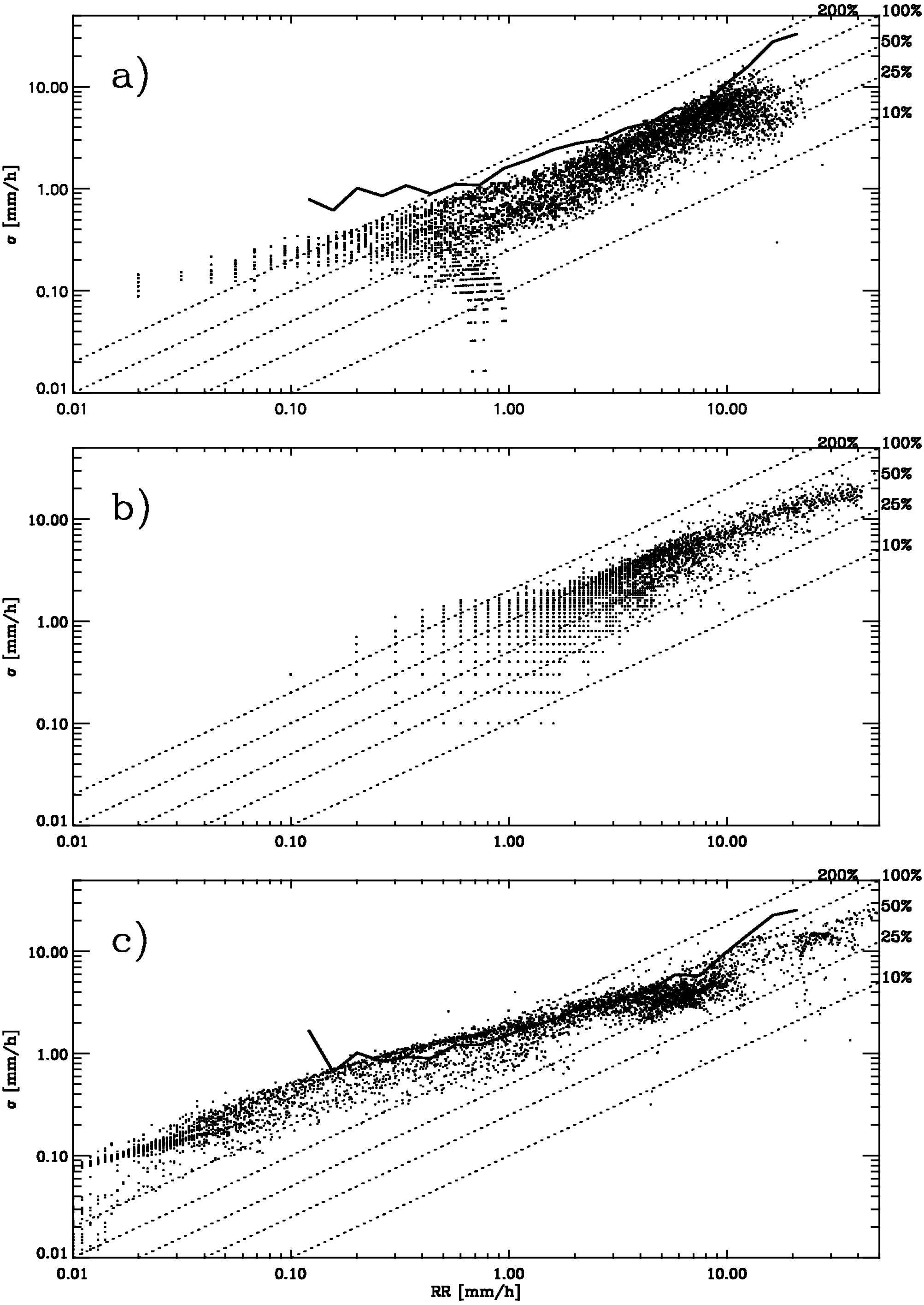

Figure 1. Bayesian retrieval errors from (6) as a function of rain rate at product resolution for (a) PATER, (b) BAMPR, and (c) 2A12 V5.1 (see text). Superimposed are solid lines denoting average differences between (a) PATER and PR and (c) 2A12 V5 and PR retrievals, respectively.

TABLE 2. CASES FOR DATA SHOWN IN FIG. 1

Date	Orbit	Centre	Rain type
PATER:			
16/12/1997	00295	(12°N, 144°E)	Cyclone 'Paka', Pacific Ocean
10/02/1998	01171	(15°S, 60°E)	Cyclone 'Anacelle', Indian Ocean
16/02/1998	01273	(5°S, 145°W)	Deep convection, Pacific Inter Tropical Convergence Zone
26/08/1998	04283	(33°N, 75°W)	Hurricane 'Bonnie', west Atlantic
29/08/1998	04328	(23°S, 142°W)	Frontal system, east Pacific
21/01/1999	06620	(3°N, 81°E)	Deep convection, Indian Ocean
02/08/2000	15438	(6°N, 16°W)	Squall line, west African coast
25/08/2000	15795	(18°N, 70°E)	Monsoon, west Indian coast
28/08/2000	15835	(13°N, 134°W)	Convection, central Pacific
30/08/2000	15876	(34°N, 72°W)	Frontal system, North American east coast
11/09/2000	16059	(35°N, 33°W)	Extratropical depression, east Atlantic
17/09/2000	16151	(3°N, 70°E)	Monsoon scattered convection, Indian Ocean
BAMPR:			
25/08/1998	04267	(30°N, 74°W)	Hurricane 'Bonnie', west Atlantic
19/08/1999	04176	(11°S, 179°W)	Convection, South Pacific Convergence Zone
24/12/1999	11938	(13°S, 71°E)	Hurricane 'Astrid', west Atlantic
2A12:			
19/12/1997	00336	(16°N, 136°E)	Supertyphoon 'Paka'

profile distributions represented in the databases (i.e. $P(\mathbf{x})$) and non-uniqueness of the TB–rainfall relationship. Another observation is that the lower limit of rain detection can be set to $\approx$0.1 mm h^{-1} because the retrieval errors are $\approx$100–200%. Below this threshold the assumption of Gaussian error distributions will not hold anymore.

As another means of validation, root-mean-square (r.m.s.) differences between TMI and PR retrievals at a unified resolution (27×40 km^2) are shown in Fig. 1 as lines superimposed on the scatterplot. The cases from which the data were computed are identical to those from the PATER Bayesian error calculation (see Table 2). Please note that the comparison to PR data covers both systematic and random errors; i.e. if the TMI estimates were to be bias-corrected by those of the PR, the resulting errors in Fig. 1 would be lower. The r.m.s. differences between PATER and PR retrievals are at the upper limit of the Bayesian errors which suggests that the retrievals are not completely unbiased; however, the magnitudes are very similar. For 2A12 V5 the r.m.s. difference to PR retrievals is almost identical to that of PATER. Since the 2A12 V5.1 Bayesian errors are a little larger than those of PATER, the curve follows well the average distribution of the data. Note, however, that the TMI–PR r.m.s. differences include random error contributions from both TMI and PR. For example, a 1 dBZ calibration error contained in the PR data would produce a retrieval error of about 15%.

5. SPATIAL AVERAGING

Before the rainfall retrievals can be assimilated into the model, spatial averaging has to be carried out to match the model resolution at which the comparison with model rain rates enters the cost function (see Marécal and Mahfouf (2002), Eq. 1). For this, the number of estimates inside the model grid, N, is needed given that this is fully included in the swath and that all these estimates are successful retrievals (including 'no rain'). This number depends on the sampling rather than the spatial resolution of the products; however, the resolution is important regarding the spatial correlation of the retrievals in each grid box, as will be discussed later, since resolution should be inversely related to spatial correlation.

BAMPR and PATER data are sampled like the lower frequency TMI channels: 104 along-scan fields of view with a separation distance of $\approx$10 km, while the distance between scan lines is roughly 14 km resulting from the velocity of the sub-satellite point and the TMI antenna rotation frequency. 2A12 data are interpolated to the locations of the 85.5 GHz channels. Thus, the along-scan separation distance reduces to $\approx$5 km while the along-track distance is identical to that of the other products. Given the model grid size used by Marécal and Mahfouf (2002), i.e. $\approx$60 km, $N_{\mathrm{2A12}} \approx 50$ and $N_{\mathrm{PATER,BAMPR}} \approx 25$, while for the current operational model version ($\approx$45 km) $N_{\mathrm{2A12}} \approx 30$ and $N_{\mathrm{PATER,BAMPR}} \approx 15$. Figure 2 illustrates both sampling and resolution for each product near the scan centre and scan edge.

If RR^{t} is the true rain rate, we can define the error of each retrieval with respect to RR^{t} at the ith pixel as $RR_i - RR_i^{\mathrm{t}}$. In our case, the random component of this error is characterized by a standard deviation σ_i, which is a function of rain rate provided by an algorithm at the ith pixel. As a variance σ_i^2, the error may either originate from the Bayesian estimator (6) or from the comparison to PR data. The standard deviation of the error in the mean rain rate $\overline{RR}$ for spatially correlated errors is

$$\sigma_{\overline{RR}} = \frac{1}{N}\left\{\sum_{i=1}^{N}\sum_{j=1}^{N} C(i,\,j)\sigma_i\sigma_j\right\}^{1/2}, \tag{7}$$

which reduces to

$$\sigma_{\overline{RR}} = \frac{1}{N}\left\{\sum_{i=1}^{N}\sigma_i^2\right\}^{1/2} \tag{8}$$

in the case of spatially uncorrelated errors because $C(i,\,j) = \delta_{ij}$.

(*a*) *Simulated effects*

To investigate the gross effects of spatial averaging, a simulation of error scaling to two different model grids was carried out. It was assumed that the entire grid box is covered with rainfall observations. Inside the box a log-normal rainfall probability distribution (pdf) was assumed with

$$P(x) = \frac{1}{\sigma_x\sqrt{2\pi}}\exp\left\{-\frac{(x-\overline{x})^2}{2\sigma_x^2}\right\}, \qquad \overline{x} = \int_{-\infty}^{\infty} xP(x)\,\mathrm{d}x, \tag{9}$$

where $x = \log(RR)$, and the associated variance $\sigma_x^2 = \overline{(x-\overline{x})^2}$. The standard deviation was assumed to be constant with $\sigma_x = \sqrt{1.21}$ following Kedem *et al.* (1990). The transfer to $\log(RR)$ was carried out to improve the integration with sparse discrete data. Thus, the scaling to model grid size is realized by an integration of rainfall-dependent errors over the rainfall probability distribution with mean $\overline{x} = \sum_{i=1}^{N} x_i P(x_i) w_i$, where the w_i represent the weights of the Gaussian quadrature at discrete x_i with $\sum_{i=1}^{N} P(x_i)w_i \approx 1$. The number of x_i is obtained from spatial sampling versus model grid-box size and the summation limits are at $\overline{x} \pm \sigma_x$. As in (7), the variance of the mean rain rate is

$$\sigma_{\overline{x}}^2 = \frac{\sum_{i=1}^{N}\sum_{j=1}^{N} P(x_i)P(x_j)w_i w_j \sigma_i\sigma_j}{(\sum_{i=1}^{N} P(x_i)w_i)^2}, \tag{10}$$

which reduces to

$$\sigma_{\overline{x}}^2 = \frac{\sum_{i=1}^{N} P(x_i)^2 w_i^2 \sigma_i^2}{(\sum_{i=1}^{N} P(x_i)w_i)^2} \tag{11}$$

for spatially uncorrelated errors. Here, σ_i is the error associated with local rain rate RR_i.

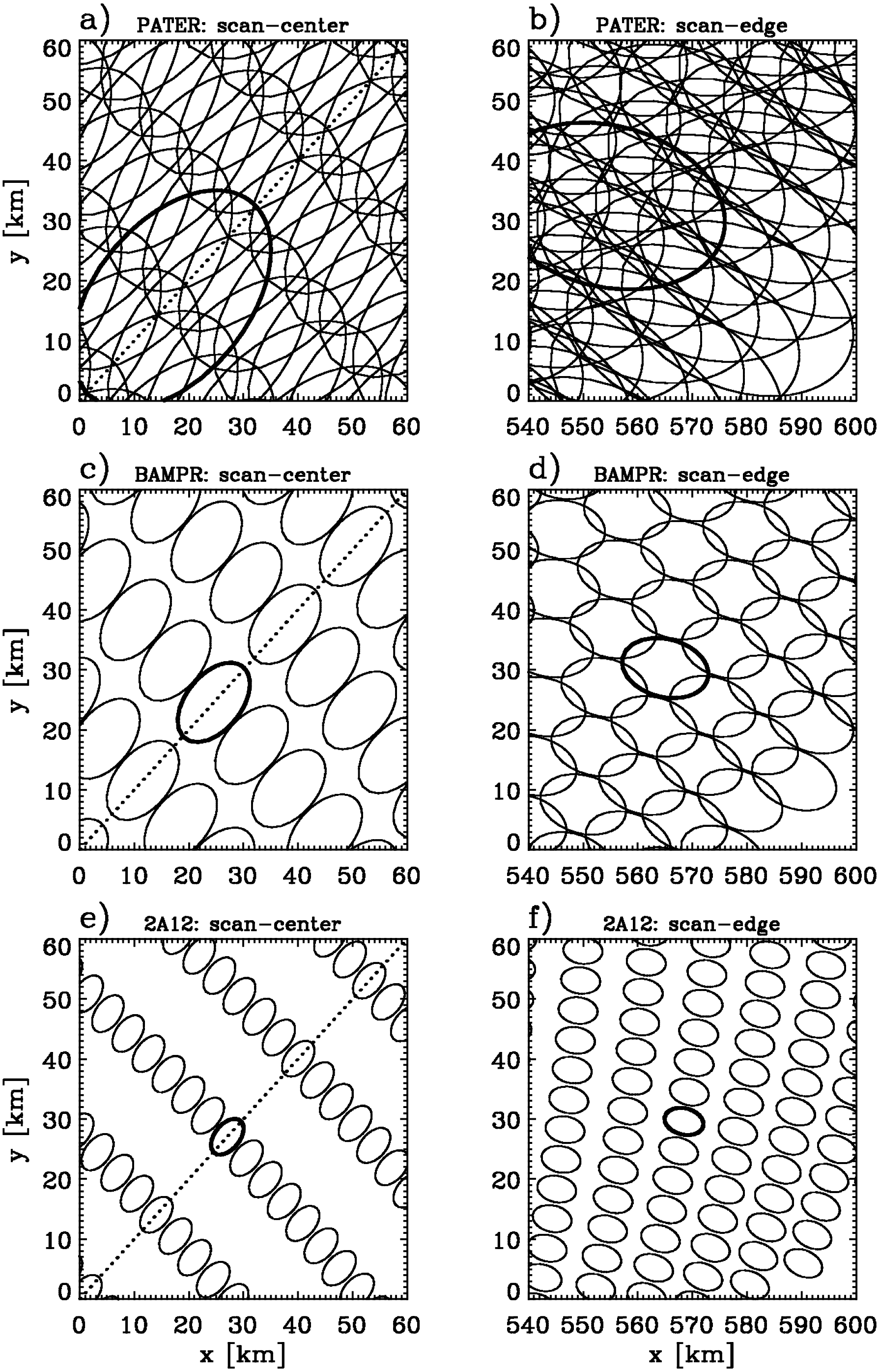

Figure 2. Example of sampling and spatial resolution of PATER near the TMI (a) scan centre and (b) scan edge. (c)–(d) and (e–f): same as (a)–(b) but for BAMPR and 2A12, respectively. See text for explanation.

To facilitate usage, error fits were derived to compute errors as a function of rain rate for all algorithms (see Fig. 3(a)). For PATER, however, not the 'Bayesian' error but the r.m.s. difference between TMI and PR retrievals, after calibrating the PATER estimates, were taken (Bauer *et al.* 2001). This is because only calibrated retrievals were used in the assimilation experiments (Marécal *et al.* 2002):

$$\begin{aligned} \sigma_{\mathrm{PATER}} &= \max(23.464 w^{0.12} \sigma_w, 0.2)\ \mathrm{mm\,h^{-1}}, \\ \sigma_w &= (0.1 + 0.45 \log_{10}(w)) w\ \mathrm{g\,m^{-3}}. \end{aligned} \tag{12}$$

Therefore, these errors are smaller than those shown in Fig. 1(a). The fit to the BAMPR data produced

$$\sigma_{\mathrm{BAMPR}} = 0.7 RR\ \mathrm{mm\,h^{-1}}, \tag{13}$$

and for 2A12 V5.1

$$\sigma_{\mathrm{2A12}} = 1.357 RR^{0.7}\ \mathrm{mm\,h^{-1}} \tag{14}$$

was obtained. Figures 3(b) and (c) present the results from applying (11) to the error curves shown in Fig. 3(a). As expected, the errors are reduced for increasing model grid-box size and the linearity of the BAMPR fit is conserved. The reduction of errors is significant and reaches 50% for 1 and 10 mm h^{-1} average rain rates on the 60 km grid. At low rain rates the errors remain at 50–100% which may point to significant rain-detection error magnitudes in the vicinity of rain clouds.

(*b*) *Data*

The evaluation of the error scaling with actual TMI retrievals was prepared by the calculation of the spatial correlations C of retrieved rain rates from each algorithm. It was assumed that these are identical to the spatial correlations of the errors. This assumption is justified in the situation where errors are proportional to rain rates. Figure 1 shows that this is reasonable between 2 and 20 mm h^{-1} for all three algorithms. TMI data covering a 6 h period (0300–0900 UTC) on 25 August 1998 were taken and within 120 km model grid boxes the spatial correlations from each algorithm were calculated. The total number of data points was between ≈20 000 and 40 000 depending on the algorithm. This range indicates already that the rain detection skill is different between the algorithms.

Figure 4 shows the results as a function of separation distance s for PATER, BAMPR and 2A12 from the data (Fig. 4(a)) and from the following fits (Fig. 4(b)):

$$\begin{aligned} C_{\mathrm{PATER}} &= a_0 + a_1 s + a_2 s^2, \\ C_{\mathrm{BAMPR}} &= \frac{\exp(-b_2\, s)}{b_0 + b_1 s}, \\ C_{\mathrm{2A12}} &= \frac{\exp(-c_2 s)}{c_0 + c_1 s}, \end{aligned} \tag{15}$$

with $a_0 = 1.0416, a_1 = -0.016082, a_2 = 7.5697\ 10^{-5}, b_0 = 0.945962, b_1 = 0.0681345$, $b_2 = 0.000735678$, $c_0 = 0.999447$, $c_1 = 0.053814$ and $c_2 = -0.00399736$. The functional form of C_{2A12} and C_{BAMPR} follows the one which was employed in the stochastic rainfall model of Bell *et al.* (1990).

Generally, with increasing distance the correlation decreases exponentially; however, the different spatial resolutions of the products are expressed by different

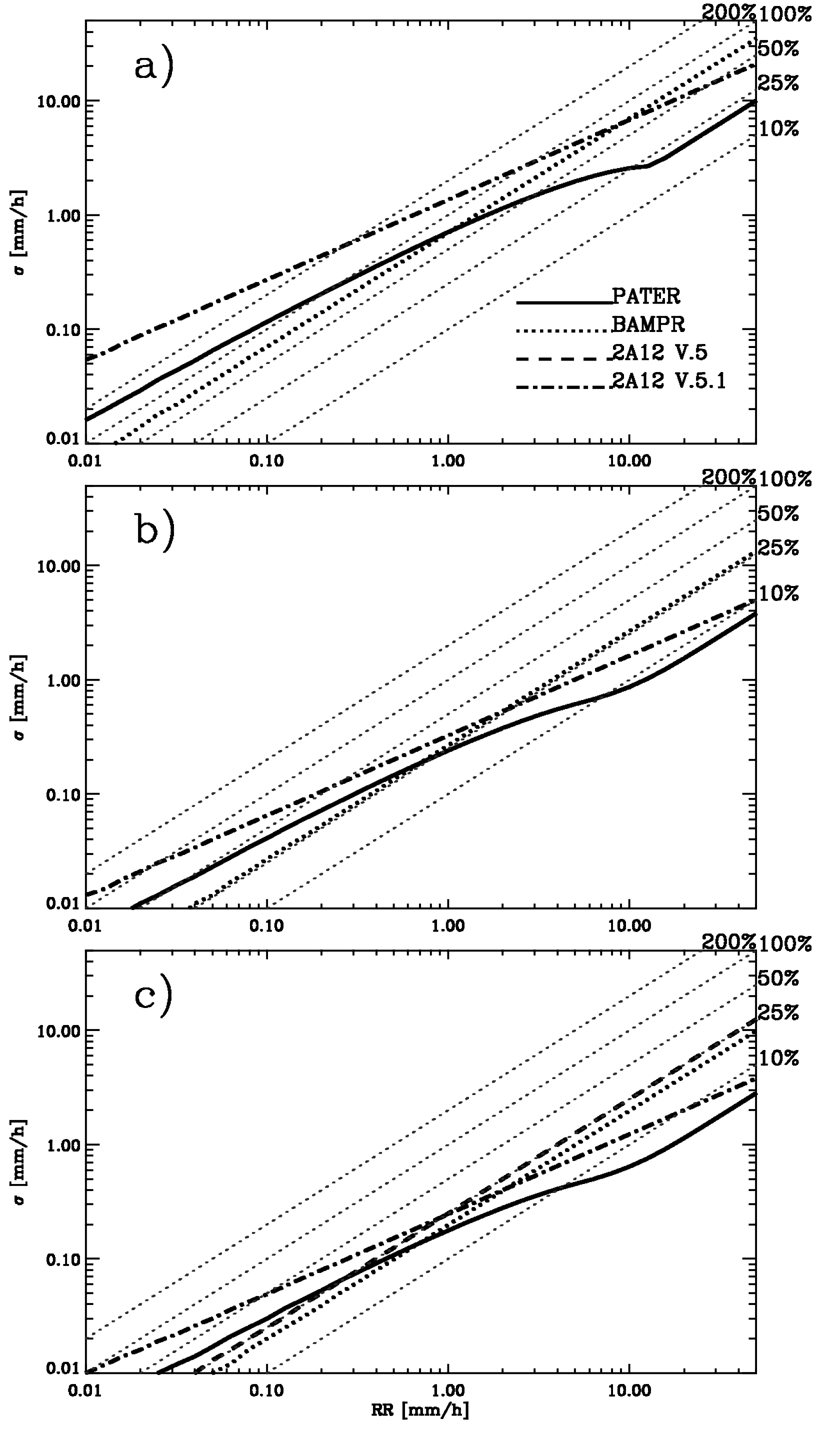

Figure 3. Error fits as a function of rain rate (a) at product resolution, (b) after spatial averaging to 45 km model grid, and (c) 60 km model grid, applying (11). The error of product 2A12 V.5 is defined for the 60 km model grid only.

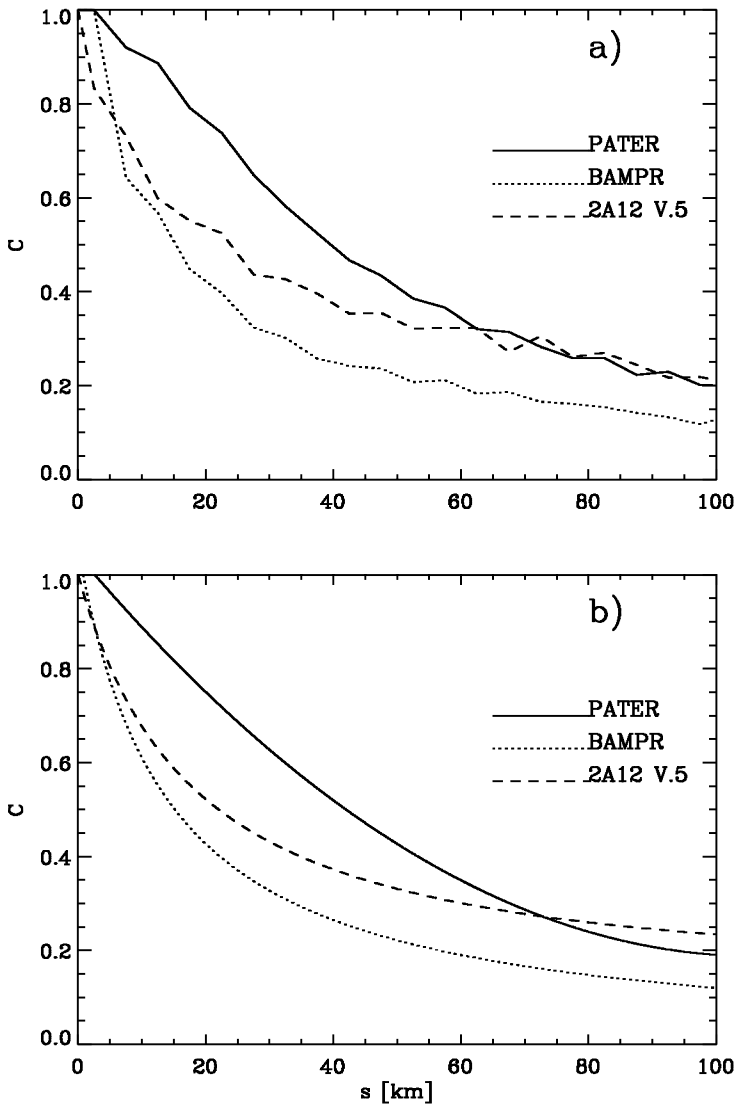

Figure 4. Spatial correlation of TMI products obtained (a) from data and (b) represented by fits in (15). See text for explanation.

gradients. Since PATER provides the lowest resolution product involving a strong overlap of neighbouring pixels (see Figs. 2(a) and (b)), a higher correlation for $s < 60$ km (where $C \approx 1/\mathrm{e}$) is noticed. This is about twice the size of the field of view and without any overlap. 2A12 shows a stronger decrease of C with s, i.e. a larger spatial variability for $s < 60$ km, while beyond 2A12 and PATER behave similarly. Despite its lower spatial resolution with respect to 2A12, BAMPR retrievals show less correlation. A possible reason is the usage of the 85.5 GHz channels in the BAMPR database which are only weakly correlated with the surface rain rate as well as the use of different drop size distributions. As a result, neighbouring retrievals may provide large differences in rainfall while TBs are still strongly correlated. Therefore, spatial resolution alone does not explain BAMPR's spatial correlation pattern. Also, the error correlation contained in the forward calculations may differ between the algorithms.

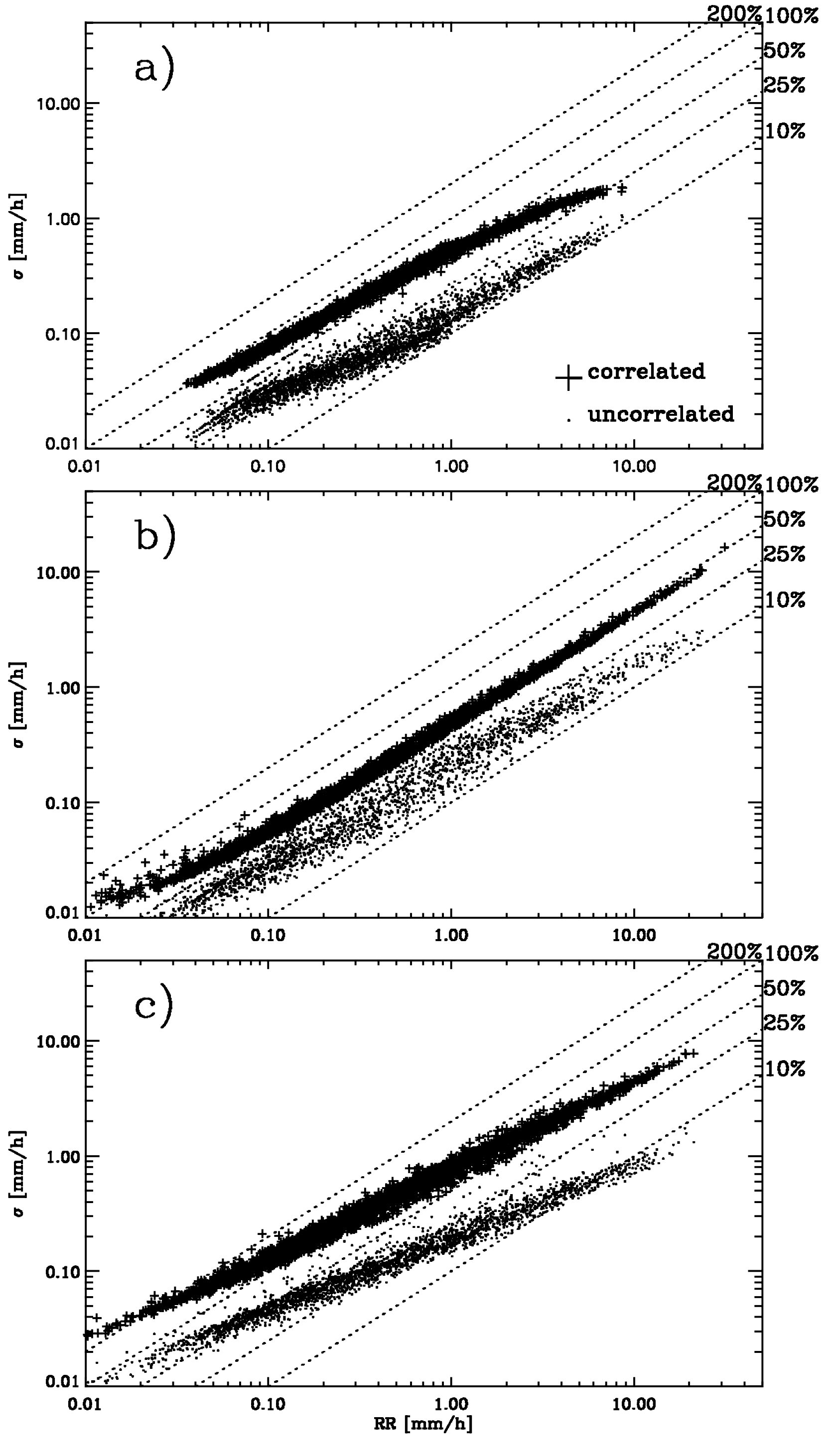

Figure 5. Errors as a function of rain rate after spatial averaging on 60 km model resolution with and without accounting for spatial correlation from (a) PATER, (b) BAMPR and (c) 2A12 V.5, over a 6 h observation period on 27 August 1998. See text for explanation.

The above correlation patterns were applied by averaging TMI retrievals from 2A12, BAMPR and PATER using the fits from Fig. 3 over the same period, i.e. applying (7) for a model grid resolution of 60 km. Please note that for 2A12 the fit given in (14) was used. As a reference, the computations were repeated without spatial correlation, i.e. using (8). Comparing the two clusters in Figs. 5(a)–(c), it is noted that the inclusion of spatial correlation causes an increase of error magnitude but a decrease of scatter. Both effects are caused by the constraint which the correlation imposes on the error compensation. In any case, the error reduction is fairly continuous and almost linear with $\log(RR)$.

The clusters of dots in Fig. 5 compare very well with the results from the error simulation, i.e. the solid, dotted, and dash-dotted lines in Fig. 3(c). Apparently, the assumption of log-normal pdfs with fixed variance holds well for averaged rain rates. In summary, including spatial correlation increases the total rain-rate errors by $\approx$50% because completely uncorrelated estimates are more efficient in random-error reduction. Since PATER shows the highest spatial correlations, its increase of errors is most pronounced. In conclusion, the influence of spatial correlation is significant but reduces the scatter. To obtain model grid-box averaged errors, the errors obtained at radiometer footprint resolution may therefore be simply scaled. This, however, depends on the algorithm performance that is the spatial correlation pattern of its rainfall estimates as a function of its nominal spatial resolution as well as the generated rain rate pdfs.

6. CONCLUSIONS

As an outcome of the EuroTRMM project, an intercomparison of retrieval errors from different TRMM passive microwave rainfall products and their propagation to average errors on global model grid-scale was carried out. All algorithms used for this study employ a Bayesian retrieval framework. The differences originate from different training databases and different probability distribution functions of retrieval variables and observables as well as individual algorithm constraints. If these products are used for variational data assimilation, error estimates are required assuming that the products are either unbiased or have been bias-corrected (with respect to the model fields). One possible output from the Bayesian algorithms is the retrieval error defined as the minimum variance solution for the errors associated with that for rain rates (or hydrometeor profiles).

Bayesian errors between 70 and 200% at low rain rates (0.1 mm h^{-1}) and between 20 and 50% at high rain rates (20–50 mm h^{-1}) were found at the original product resolution and sampling. The large errors at low rain rates originate from the large contribution of information to the signal from effects which are not directly related to rainwater, that is surface effects and non-raining cloud emission. As an example, the large errors at low rainfall rates shown in Fig. 1(c) represent surface effects since very high wind speeds were reported in the vicinity of typhoon Paka. In the middle range (1–20 mm h^{-1}), TBs are more sensitive to rainwater which reduces the direct retrieval error. However, the variability inside the database is large, which means that the ambiguity of the TB to rain-rate relation is high. Therefore, there are many possible solutions having the same TBs. At high rain rates, this variability decreases again since extreme events are usually not well covered in the databases. On the other hand, the strong contribution from precipitating ice increases the direct rain-rate retrieval error so that the net effect is the same as for moderate rainfall. Generally, the errors appear to depend linearly on $\log_{10}(RR)$. Therefore their characterization in terms of $\log_{10}(RR)$ may be useful, and this also facilitates their interpretation at low rain rates.

An independent evaluation was carried out by comparing TMI estimates to PR retrievals at the same resolution (27×40 km^2). Interestingly, the results indicate errors very similar to those obtained from the Bayesian estimator. An important qualification is that TMI–PR errors contain both systematic and random contributions while the Bayesian error estimates are assumed to be random only. A possible interpretation of error decomposition would be that at low rain rates the error consists mainly of a bias, while at moderate rain rates the random component is dominant.

Two different evaluations of the impact of spatial averaging on global model grid-scales were carried out to estimate the errors to be introduced into a variational data assimilation system, as outlined in Treadon (1997) or Marécal and Mahfouf (2002), for example. The first evaluation used the error fits from a set of case-studies (Fig. 3). Assuming spatially uncorrelated errors and realistic probability distribution functions of rain, the errors reduced to 30–50% at low rain rates and to 5–30% at high rain rates. The second evaluation used TMI observations on the ECMWF model grid. First, the spatial correlation of each data product was calculated since the number of observations inside a model grid box depends only on the data sampling and not the spatial resolution. The spatial correlation patterns reflected the product resolution (e.g. overlap of neighbouring pixels) very well. PATER produced the weakest decrease of correlation with separation distance. BAMPR retrievals showed the strongest decrease even though its spatial resolution is between that of PATER and 2A12. This is likely due to the usage of the 85 GHz channels in the retrieval algorithms and a less homogeneous database. These factors may cause larger local gradients in retrieved rain rates than obtained from the other algorithms.

Finally, the error spatial correlations were used to calculate 60 km model grid-box averaged errors as in the previous exercise. The previously modelled reduction of errors is partly compensated by the error spatial correlations. The differences between algorithms become slightly spread since their correlation patterns are different. The final error estimates ranged from 50–150% at low rain rates to 20–50% at high rain rates. Neglecting spatial correlation further reduced the errors to 20–50% at low rain rates and to 5–20% at high rain rates. The modelled and observed behaviour of spatially uncorrelated error propagation agreed well where observed and modelled rain rate pdfs were similar. An important conclusion is that once the spatial correlation pattern of a product is known, the probability density distribution of real observations inside the model grid does not produce larger scatter. This suggests that a simple scaling may suffice to calculate the error reduction to obtain an average error on the model grid.

Aiming at the direct assimilation of rain-affected radiances, the issue of grid-box averaged radiances has to be solved differently because the relationship between hydrometeor profiles and TBs is highly nonlinear. Therefore, the TB of an averaged profile is not identical with the averaged TBs of subgrid-scale profiles. Chevallier and Bauer (2002) have shown that the grid-box averaged TBs are very sensitive to the model assumption on cloud overlap and its implementation in the radiative-transfer model. Once this problem is solved the calculation of associated modelling errors is rather straightforward.

ACKNOWLEDGEMENTS

This project was funded by the European Space Agency, contract No. 12651/97/NL/NB. The authors gratefully acknowledge the usage of TRMM data which was made available through the TRMM program by the National Aeronautics and Space Administration. We are also very grateful to the three referees who provided very useful suggestions for the improvement of this article.

REFERENCES

Bauer, P. 2001 Over-ocean rainfall retrieval from multi-sensor data of the Tropical Rainfall Measuring Mission (TRMM). Part I: Design and evaluation of inversion databases. *J. Ocean. Atmos. Tech.*, **18,** 1315–1330

Bauer, P., Amayenc, P., Kummerow, C. D. and Smith, E. A. 2001 Over-ocean rainfall retrieval from multi-sensor data of the Tropical Rainfall Measuring Mission (TRMM). Part II: Algorithm implementation. *J. Ocean. Atmos. Tech.*, **18,** 1838–1855

Bell, T. L., Abdullah, A., Martin, R. L. and North, G. R. 1990 Sampling errors for satellite-derived tropical rainfall: Monte Carlo study using a space–time stochastic model. *J. Geophys. Res.*, **95,** 2195–2205

Chevallier, F. and Bauer, P. 2002 Model rain and clouds over oceans: Comparison with SSM/I observations. *Mon. Weather Rev.* (in press)

Kedem, B., Chiu, L. S. and North, G. R. 1990 Estimation of mean rain rate: Application to satellite observations. *J. Geophys. Res.*, **95,** 1965–1972

Kummerow, C. D., Olson, W. S. and Giglio, L. 1996 A simplified scheme for obtaining precipitation and vertical hydrometeor profiles from passive microwave sensors. *IEEE Trans. Geosci. Remote Sensing*, **34,** 1213–1232

Kummerow, C. D., Barnes, W., Kozu, T., Shiue, J. and Simpson, J. 1998 The Tropical Rainfall Measuring Mission (TRMM) sensor package. *J. Atmos. Ocean. Tech.*, **15,** 809–817

Kummerow, C. D., Hong, Y., Olson, W. S., Yang, S., Adler, R. F., McCollum, J., Ferraro, R. R., Petty, G. W., Shin, D.-B. and Wilheit, T. T. 2001 The evolution of the Goddard Profiling Algorithm (GPROF) for rainfall estimation from passive microwave sensors. *J. Appl. Meteorol.*, **40,** 1801–1820

Lorenc, A. C. 1986 Analysis methods for numerical weather prediction. *Q. J. R. Meteorol. Soc.*, **112,** 1177–1194

Marzano, F. S., Mugnai, A., Panegrossi, G., Pierdicca, N., Smith, E. A. and Turk, J. 1999 Bayesian estimation of precipitating cloud parameters from combined measurements of spaceborne microwave radiometer and radar. *IEEE Trans. Geosci. Remote Sensing*, **37,** 596–613

Marécal, V. and Mahfouf, J.-F. 2000 Variational retrieval of temperature and humidity profiles from TRMM precipitation data. *Mon. Weather Rev.*, **128,** 3853–3866

2002 Four-dimensional variational assimilation of total columnar water vapor in rainy areas. *Mon. Weather Rev.*, **130,** 43–58

Marécal, V., Mahfouf, J.-F. and Bauer, P. 2002 Comparison of TMI rainfall estimates and their impact on four-dimensional variational assimilation. *Q. J. R. Meteorol. Soc.* (in press)

Mugnai, A., di Michele, S., Marzano, F. S. and Tassa, A. 2001 'Cloud model based Bayesian techniques for precipitation profile retrieval from TRMM microwave sensors'. Pp. 323–346 in Proceedings of EuroTRMM workshop on assimilation of clouds and precipitation in NWP models, November 2000, Reading, UK. ECMWF, Reading, UK

Olson, W. S., Kummerow, C. D., Heymsfield, G. M. and Giglio, L. 1996 A method for combined passive–active microwave retrievals of cloud and precipitation profiles. *J. Appl. Meteorol.*, **35,** 1763–1789

Panegrossi, G., Dietrich, S., Marzano, F. S., Mugnai, A., Smith, E. A., Xiang, X., Tripoli, G. J., Wang, P. K. and Poiares Baptista, J. P. V. 1998 Use of cloud model microphysics for passive microwave-based precipitation retrieval: Significance of consistency between model and measurement manifolds. *J. Atmos. Sci.*, **55,** 1644–1673

Rabier, F., Jaervinen, H., Klinker, E., Mahfouf, J.-F. and Simmons, A. 2000 The ECMWF operational implementation of four-dimensional variational assimilation. Part I: Experimental results with simplified physics. *Q. J. R. Meteorol. Soc.*, **126,** 1143–1170

Rodgers, E., Olson, W. S., Halverson, J., Simpson, J. and Pierce, H. 2000 Environmental forcing of Supertyphoon Paka's (1997) latent heat structure. *J. Appl. Meteorol.*, **39,** 1983–2006

Tassa, A., Di Michele, S., Mugnai, A., Marzano, F. and Poiares Baptista, J. P. V. 2002 Cloud-model based Bayesian technique for precipitation profile retrieval from TRMM microwave imager. *Radio Sci.* (in press)

Treadon, R. E. 1997 'Assimilation of satellite derived precipitation estimates with the NCEP GDAS'. PhD Dissertation, Florida State University